

- were able to realize the transformation from 1-dH to tetragonal for the 3 weight % Brij-56 specimen.
34. P. Coudray, J. Chisham, M. P. Andrews, S. I. Najafi, *Opt. Eng.* **36**, 1234 (1997).
 35. G. C. Frye, A. J. Ricco, S. J. Martin, C. J. Brinker, *Mat. Res. Soc. Symp. Proc.* **121**, 349 (1988).
 36. We thank C. Braunbarth for discussions about the

phase transformation, R. Assink for assistance with NMR experiments, and Y. Guo for assistance with TEM. Partially supported by the University of New Mexico/NSF Center for Micro-Engineered Materials, Fonds zur Foerderung der Wissenschaftlichen Forschung Austria, the U.S. Department of Energy (DOE) Basic Energy Sciences Program, and Sandia

National Laboratory's Laboratory Directed R&D program. This work was done under contract from DOE. Sandia is a multiprogram laboratory operated by Sandia Corporation, a Lockheed Martin Company, for DOE under contract DE-AC04-94AL85000.

7 June 2000; accepted 16 August 2000

Vibrational Promotion of Electron Transfer

Yuhui Huang,¹ Charles T. Rettner,² Daniel J. Auerbach,²
Alec M. Wodtke¹

By using laser methods to prepare specific quantum states of gas-phase nitric oxide molecules, we examined the role of vibrational motion in electron transfer to a molecule from a metal surface free from the complicating influence of solvation effects. The signature of the electron transfer process is a highly efficient multiquantum vibrational relaxation event, where the nitrogen oxide loses hundreds of kilojoules per mole of energy on a subpicosecond time scale. These results cannot be explained simply on the basis of Franck-Condon factors. The large-amplitude vibrational motion associated with molecules in high vibrational states strongly modulates the energetic driving force of the electron transfer reaction. These results show the importance of molecular vibration in promoting electron transfer reactions, a class of chemistry important to molecular electronics devices, solar energy conversion, and many biological processes.

The prototypical process of electron transfer is one of the most fundamental elementary chemical reactions found in nature. The pioneering work of Marcus (1) has exploded into a vigorous field of chemical and biochemical research, which has been recently reviewed (2). Electron transfer rates are controlled by two central dynamics: "solvent polarization" and "intramolecular vibrational motion." Under certain circumstances, it is the reorganization of the polarizable solvent about the moving charge that controls the rate of reaction (1). Under other circumstances, the electron transfer rate can only be understood by including effects of intramolecular vibration either classically (3) or quantum mechanically (4–6). Although hybrid models that incorporate both effects have recently been developed (7–11), our understanding of the dynamics of this important process is still far from complete. Furthermore, although studies of solvent influences on electron transfer have been quite successful (12, 13), the difficulties of performing state-resolved experiments in condensed phases have limited experiments on vibrational influences (14).

We found a way to at once remove the complicating effects of the solvent and to control the vibrational state of the reacting molecule by studying electron transfer dynamics between an incident gas molecule and a metal surface. This model system is in many ways

dynamically equivalent to condensed phase electron transfer, but solvent effects appear in a much simpler way. Specifically, the interaction of the ion with the solvent is replaced by an interaction with its image charge in the metal, which is much more easily modeled (15, 16). Furthermore, this approach allows the application of gas-phase optical pumping to prepare single quantum states in very high vibrational states in order to amplify the possible effects of vibration on electron transfer. We show that high levels of vibrational excitation can promote electron transfer from a metal surface to a gas-phase molecule. This work builds on previous condensed phase studies that have revealed substantial enhancements of electron transfer rates with vibrational excitation (14)

and provides a model system for the development of sophisticated charge transfer theories.

Electron transfer rates depend on molecular vibration because the shape of the molecule changes upon charge transfer. Classically, trajectories of vibrationally excited states can more easily traverse regions of configuration space similar to the stable anion. For the case of NO, we quantitatively calculated the form of the relevant molecular potentials (17) (Fig. 1A).

The difference between the two potential functions (Fig. 1B) is the vertical electron binding energy versus N–O separation. Near their potential minima, there is little energy difference between the neutral and anion curves, consistent with the low electron affinity associated with NO. For vibrationally excited states, however, near the outer turning point of the vibration state $\nu = 15$ (bond length $R_{\text{NO}} \sim 1.6$ Å), the vertical attachment energy to form NO^- is >200 kJ/mol. At the inner turning point, electron attachment is endoergic by about the same amount. This simple analysis shows that the energetic constraints controlling the ability of NO to accept (or, concomitantly, the ability of NO^- to donate) electrons depend strongly on internuclear separation.

Previously, News derived potential parameters for neutral and anionic curves that describe the interaction of NO with Ag(111) (16). These are shown in Fig. 2, adapted to the case of Au(111). The anionic curve is calculated by using a Coulombic interaction between the anion and the image charge of the metal. The neutral curve reflects the weak physical interactions of NO with the noble metals. The asymptotic separation between the neutral and

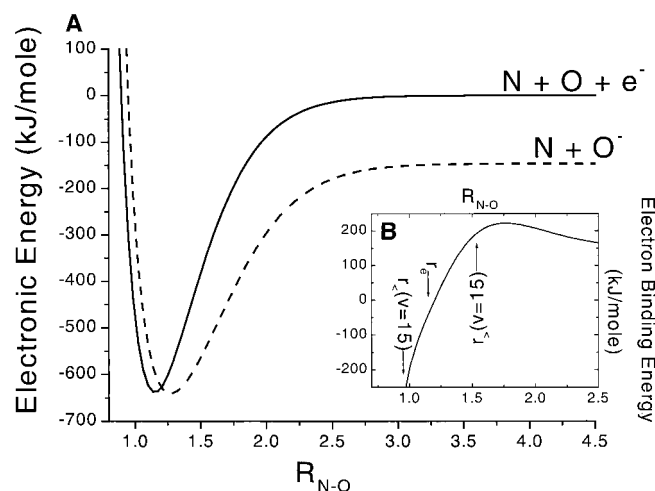


Fig. 1. (A) Ab initio calculations of NO and NO^- , showing the energetic constraints on electron transfers. (B) The difference between the two potential curves. The positions of the inner and outer extrema of the NO ($\nu = 15$) vibrational wave function are shown with vertical arrows labeled (r_+ and r_-). The position of the NO potential minimum is shown as r_e .

¹Department of Chemistry, University of California, Santa Barbara, CA 93106, USA. ²IBM Research Division, Almaden Research Center, San Jose, CA 95120–6099, USA.

Fig. 2. Newn's electron-mediated interactions of NO with a metal (M). This figure is based on the analysis of (16). The x axis indicates the distance from the surface to the O atom. (A) The NO molecule is held at its equilibrium bond length. The asymptotic energy separation is given by the difference between the surface work function and the electron binding strength to the NO. This results in a substantial barrier to electron transfer for NO on Au. (B) Same as (A), but the NO bond length has been extended to 1.6 Å, close to the outer classical turning point of NO ($\nu = 15$). The enhanced electron binding strength of NO now causes the barrier to electron transfer to disappear.

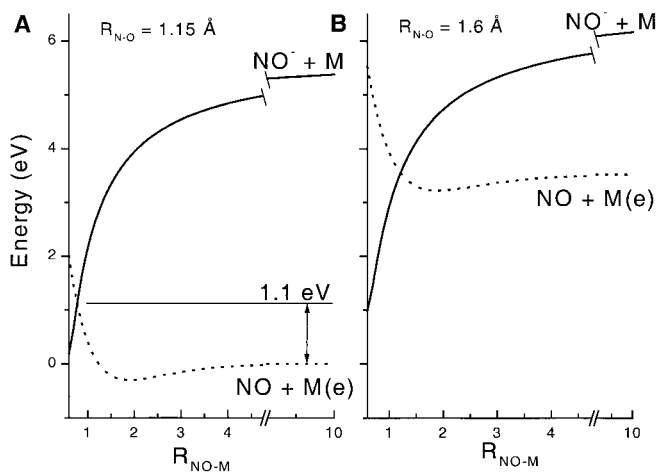
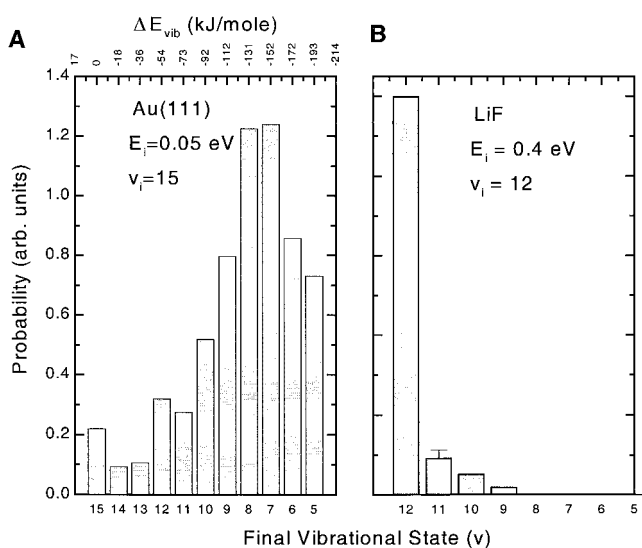


Fig. 3. Measured vibrational distribution of NO resulting from the scattering of (A) NO ($\nu = 15$) from Au(111) at $E_i = 5$ kJ/mol and (B) NO ($\nu = 12$) from LiF at $E_i = 38$ kJ/mol.



anionic potentials is given by the difference between the surface work function and the NO electron binding energy. Figure 2A shows the expected potentials when NO is held at its equilibrium bond length. A barrier to the curve crossing arises, which has been used to quantitatively explain the strong incidence energy dependence for vibrational excitation (16) observed in experiment (18). When NO is held at a bond length of 1.6 Å (near the outer turning point of $\nu = 15$), the enhanced electron binding energy represented in Fig. 1 shifts the two potentials with respect to one another. Thus, for conditions where large-amplitude vibrational motion allows access to NO bond lengths on the order of 1.5 Å, the barrier to charge transfer is eliminated (19). In light of this, we expect that the excitation of NO to such highly vibrationally excited states should massively enhance the electron transfer probability at low incidence energies. We now present experiments capable of observing this behavior (20).

Detection of the electron transfer product is complicated by the inability of NO^- to escape the surface (Fig. 2). Despite this, the electron transfer process provides a striking signature in this experiment, in the form of a uniquely efficient mechanism for vibrational relaxation. NO scattered back from the surface in various spin-rotation-vibration states is state-specifically and resonantly ionized by a third pulsed dye laser operating at 270 to 350 nm. An in-line microchannel plate-based detector detects these ions.

The measured vibrational distribution derived from our experiments when NO ($\nu = 15$) is scattered from the Au(111) surface at an incidence energy of only 5 kJ/mol (21) is shown in Fig. 3A. Only a few percent or less of the observed scattering flux emerged in the initial vibrational state (22). Equally striking is the fact that the most probable scattered vibrational state results from a loss of seven to eight vibrational quanta representing ~ 150 kJ/mol of energy.

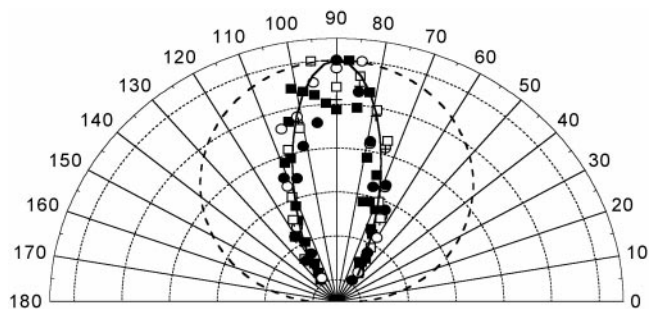
Electron transfer has been a subject of much discussion concerning the interactions of vibrationally excited molecules with metal surfaces (16, 18, 23–27). Vibrational excitation of polyatomic molecules colliding with metal surfaces is thought to involve relaxation of thermally excited electron-hole pairs by a mechanism involving electron transfer (16, 18, 26). Experiments (27) consistent with theoretical predictions (28) of the incidence energy dependence of survival probability of vibrationally excited molecules in collisions with metals provide additional evidence that electron transfer is important in the scattering of polyatomics from metals.

To see how electron transfer can cause this high degree of relaxation observed in this work, we need to appreciate two points. First, the product NO^- species has a substantially different diatomic potential and will be formed in a range of different vibrational states. Second, by the time the electron jumps back to the surface, the molecular anion will be at a different vibrational phase, which will favor different vibrational states for the neutral NO. These ideas were discussed in detail by Gadzuk and Holloway (24, 29, 30) in the context of the reverse process of excitation. The key point is that the transitions from the neutral to ionic surfaces and back can lead to very large changes in the NO vibrational state, resulting in a highly efficient mode of vibrational relaxation. Furthermore, the experiments show that this can happen at a very low incidence energy.

These observations stand in contrast to purely mechanical gas-surface vibrational relaxation, which is known to be very inefficient for the large vibrational spacings found in small molecules (31, 32). Studies of the vibrational relaxation of small molecules on insulating surfaces have found that relaxation occurs on a millisecond time scale, indicating that vibration couples very weakly to phonons of the solid (33–35). To pursue this point further, we examined the vibrational relaxation of NO ($\nu = 12$) at an insulating LiF surface. The vibrational distribution of the scattered molecules is shown in Fig. 3B and appears in stark contrast to the results from Au(111) (36). We find that, for NO ($\nu = 12$), there is almost no vibrational relaxation at any incidence energies we studied.

In the electron-jump model of multiquantum vibrational relaxation, we would expect the vibrational energy to be transferred to the electronic energy of the substrate rather than to other motions of the NO. Our measurements of the rotational and translational distributions of the scattered NO are consistent with this picture. Rotational distributions of the scattered NO made with state-resolved resonance enhanced multiphoton ionization (REMPI) reveal that the rotational excitation for molecules undergoing the efficient multiquantum vibrational relaxation is about the same as that for vibrationally elastic scattered NO ($\nu = 0$) and that the rota-

Fig. 4. Angular distribution of product scattering channels resulting from incident NO ($v = 15$) on Au(111). Symbols represent the following: solid squares, $\Delta v = -4$, $E_i = 5$ kJ/mol; open circles, $\Delta v = -7$, $E_i = 29$ kJ/mol; crosses, $\Delta v = -5$, $E_i = 29$ kJ/mol; open squares, $\Delta v = -4$, $E_i = 29$ kJ/mol; and solid circles, $\Delta v = -2$, $E_i = 29$ kJ/mol. Also shown are $\cos^{14} \Theta$ (solid line) and $\cos \Theta$ (dashed line).



tional excitation does not depend strongly on the change in vibration state Δv . Clearly, little of the energy available from the vibrational relaxation is appearing as rotational excitation of the scattered products. We also carried out time-of-flight (TOF) measurements of the scattered molecules (37) and found no evidence that the vibrational relaxation energy is appearing as a translation of the scattered NO.

We estimate that the multiquantum vibrational energy transfer occurs on the subpicosecond time scale, based on measurements of the differential scattering cross section (Fig. 4) (38). The solid line passing through the data points represents $\cos^{14} \Theta$ (Θ is the exit angle from the surface normal). The scattering angular distributions provide powerful evidence that the various vibrational channels result from a specular (direct scattering) mechanism. Should the molecules spend any appreciable time adsorbed on the surface, we would expect the angular distribution to broaden to a $\cos \Theta$ distribution, as shown by the dashed line. With the through-space electron transfer distance consistent with the potential surfaces of Fig. 2, classical trajectory calculations on realistic potentials give the best estimate of the time scale of a direct scattering mechanism (39). Using the velocity of NO at an incidence energy $E_i = 0.05$ eV, we find a scattering time of 0.1 ps. The fact that such large amounts of vibrational energy can be transferred from the NO molecule to the metal surface on such a short time scale is again strong evidence for an electron-mediated process.

Another point of contrast between metal and insulator scattering experiments is in the vibrational dependence of the survival probability. Direct measurements of the survival probability of NO ($v = 12$) scattering from LiF vary between 70 and 90% ($\pm 10\%$), increasing modestly with incidence energy, and are similar to values derived from NO in $v = 1$ (32). In contrast, for NO (v) on Au(111), the survival probability (at $E_i = 5$ kJ/mol) drops from $>95\%$ for $v = 2$ (27) to less than a few percent for $v = 12$ and 15.

A key aspect of the present work is the fact that the electron transfer probability (and concomitant vibrational relaxation) is enhanced by large-amplitude vibration and that

the influence of vibration is much more subtle than simply enhancing Franck-Condon factors between reactant and product. As has been discussed in theoretical treatments of electron transfer, vibrational excursions can modulate the energetic barriers to electron transfer. To clarify this point, we compare our results to recent measurements of the incidence energy dependence of vibrational excitation and de-excitation of NO ($v = 2$) under conditions otherwise identical to our present study. For NO ($v = 2$), the Franck-Condon factor with NO^- ($v = 0$) is 0.5, twice that for NO ($v = 0$). Despite this, experiments show that, for NO ($v = 2$) on Au(111), electron transfer is unimportant at the low incidence energies reported here (27). In other words, it is not the change in Franck-Condon factors that turns on the electron transfer for NO ($v = 15$), but rather the large change in electron transfer energetics accompanying large-amplitude vibrational motion. We think that this behavior may be of general importance to electron transfer rates.

References and Notes

1. R. A. Marcus, *Annu. Rev. Phys. Chem.* **15**, 155 (1964).
2. N. Sutin, in *Electron Transfer—From Isolated Molecules to Biomolecules, Part 1*, J. Jortner and M. Bixon, Eds., vol. 106 of *Advances in Chemical Physics* (Wiley, New York, 1999), pp. 7–33.
3. H. Sumi and R. A. Marcus, *J. Chem. Phys.* **84**, 4272 (1986).
4. N. R. Kestner, J. Logan, J. Jortner, *J. Phys. Chem.* **78**, 2148 (1974).
5. S. Efrima and M. Bixon, *Chem. Phys. Lett.* **25**, 34 (1974).
6. ———, *Chem. Phys.* **13**, 447 (1976).
7. G. C. Walker, E. Akesson, A. E. Johnson, N. E. Levinger, P. F. Barbara, *J. Phys. Chem.* **96**, 3728 (1992).
8. D. K. Phelps and M. J. Weaver, *J. Phys. Chem.* **96**, 7187 (1992).
9. N. Gayathri and B. Bagchi, *J. Phys. Chem. A* **103**, 8496 (1999).
10. B. Bagchi and N. Gayathri, in *Electron Transfer—From Isolated Molecules to Biomolecules, Part 2*, J. Jortner and M. Bixon, Eds., vol. 107 of *Advances in Chemical Physics* (Wiley, New York, 1999), pp. 1–80.
11. P. F. Barbara, T. J. Meyer, M. A. Ratner, *J. Phys. Chem.* **100**, 13148 (1996).
12. M. A. Kahlow, W. Jarzaba, K. Tai Jong, P. F. Barbara, *J. Chem. Phys.* **90**, 151 (1989).
13. K. Tai Jong, W. Jarzaba, P. F. Barbara, T. Fonseca, *Chem. Phys.* **149**, 81 (1990).
14. K. G. Spears, X. N. Wen, R. H. Zhang, *J. Phys. Chem.* **100**, 10206 (1996).
15. J. W. Gadzuk, *J. Chem. Phys.* **79**, 6341 (1983).
16. D. M. News, *Surf. Sci.* **171**, 600 (1986).
17. The NO potential has been derived from spectroscopic data and previously reported in an analytical form [P. Huxley and J. N. Murrell, *J. Chem. Soc. Faraday Trans. 2* **79**, 323 (1983)]. Ab initio calculations of the NO^- potential have also been reported [M. Corneliuss-McCarthy, J. W. R. Allington, K. S. Griffith, *Chem. Phys. Lett.* **289**, 156 (1998)]. Figure 1 shows an optimized analytic function that fits the ab initio points to better than 6 kJ/mol. A small constant energy offset to the negative ion potential (<10 kJ/mol) was introduced in Fig. 1 to accurately reflect the known O-atom electron affinity reported by D. M. Neumark, K. R. Lykke, T. Andersen, and W. C. Lineberger [*Phys. Rev. A* **32**, 1890 (1985)].
18. C. T. Rettner, F. Fabre, J. Kimman, D. J. Auerbach, *Phys. Rev. Lett.* **55**, 1904 (1985).
19. At the inner turning point of NO vibration, the barrier to electron transfer is raised to >450 kJ/mol.
20. The methods used here are very similar to those reported by H. Hou *et al.* [*Science* **284**, 1647 (1999)]. Briefly, a nanosecond-pulsed dye laser was used together with nonlinear optics to generate light at 204.7 nm. With this light, we excite NO ($v = 0$, $J = 0.5$), where J is the rotational state, in its ground electronic state up to the $A^2\Sigma^+$ ($v = 2$, $J = 0.5$) state. Another pulsed dye laser (overlapped in space and time) operates at 422.8 nm and stimulates emission from $A^2\Sigma^+$ ($v = 2$, $J = 0.5$) back down to the ground electronic state, populating, for example, NO ($v = 15$, $J = 0.5$). In this experiment, we are able to control the initial quantum state (including vibrational, rotational, spin, and parity quantum numbers) and the kinetic energy of incidence.
21. Great care was taken to derive the vibrational population distribution from the measured REMPI spectra. Fortunately, many properties of the scattered molecules do not depend on Δv , including: angular and TOF distributions, and even rotational distributions are only weakly varying with Δv . Relative REMPI signals originating from neighboring vibronic bands in the A-X system of NO were saturated by the probe laser, so that no correction for varying Franck-Condon factors in the detection step were needed. Relative vibrational-state-specific detection efficiencies were measured by preparing controlled vibrational population distributions of highly vibrationally excited NO. These distributions were prepared by spontaneous emission from laser-prepared vibrational levels of the A state of NO. The relative populations of different vibrational states can then be calculated precisely.
22. Because we were unable to observe a scattering signal emerging in vibrational states below $v = 5$ and because we cannot rule out the possibility that a fraction of the unseen NO adsorbed to the surface, this is an upper limit to the actual vibrationally elastic scattering probability.
23. J. W. Gadzuk, *Phys. Rev. Lett.* **76**, 4234 (1996).
24. S. Holloway and J. W. Gadzuk, *Surf. Sci.* **152**, 838 (1985).
25. Z. Kirson, R. B. Gerber, A. Nitzan, M. A. Ratner, *Surf. Sci.* **151**, 531 (1985).
26. E. K. Watts, J. L. W. Siders, G. O. Sitz, *Surf. Sci.* **374**, 191 (1997).
27. Y. Huang, A. M. Wodtke, H. Hou, C. T. Rettner, D. J. Auerbach, *Phys. Rev. Lett.* **84**, 2985 (2000).
28. A. Gross and W. Brenig, *Surf. Sci.* **289**, 335 (1993).
29. J. W. Gadzuk and S. Holloway, *Phys. Scr.* **32**, 413 (1985).
30. ———, *Phys. Rev. B* **33**, 4298 (1986).
31. R. R. Lucchese and J. C. Tully, *J. Chem. Phys.* **80**, 3451 (1984).
32. J. Misewich, H. Zacharias, M. M. T. Loy, *Phys. Rev. Lett.* **55**, 1919 (1985).
33. H.-C. Chong and G. E. Ewing, *Phys. Rev. Lett.* **65**, 2125 (1990).
34. G. E. Ewing, *Acc. Chem. Res.* **25**, 292 (1992).
35. A. C. Wight and R. E. Miller, *J. Chem. Phys.* **109**, 8626 (1998).
36. About 2% of the population in $v = 12$ initially undergoes infrared emission populating lower vibrational states. The reported distribution has not been corrected for this effect.
37. This is accomplished by moving the probe laser beam ~ 1.5 cm from the Au(111) surface and observing the

- signal intensity as a function of time delay between the preparation and detection laser pulses.
38. The angular distribution is found by systematically translating the probe laser beam parallel to the surface at a distance of ~ 2 cm.
39. The average kinetic energy during the collision is ~ 2000 m/s, due to the strongly attractive anionic potential.

40. We are very grateful to the Air Force Office of Scientific Research, which has supported this research even in the most difficult times, and to the Santa Barbara Laser Pool, funded by the NSF, which provided equipment essential to this work. We are also grateful for the contributions of H. Hou for his development of electron transfer models and for many stimulating discussions during the

early phases of this work. A.M.W thanks K. O. Sullivan, who was and continues to be extremely helpful with ab initio calculations. We all express special thanks to J. Brauman, who was a wonderful sounding board in the early stages of manuscript preparation.

6 June 2000; accepted 18 August 2000

Dynamically Controlled Protein Tunneling Paths in Photosynthetic Reaction Centers

Ilya A. Balabin and José N. Onuchic*

Marcus theory has explained how thermal nuclear motions modulate the energy gap between donor and acceptor sites in protein electron transfer reactions. Thermal motions, however, may also modulate electron tunneling between these reactions. Here we identify a new mechanism of nuclear dynamics amplification that plays a central role when interference among the dominant tunneling pathway tubes is destructive. In these cases, tunneling takes place in protein conformations far from equilibrium that minimize destructive interference. As an example, we demonstrate how this dynamical amplification mechanism affects certain reaction rates in the photosynthetic reaction center and therefore may be critical for biological function.

Electron transfer (ET) reactions play a key role in living systems, particularly in bioenergetic pathways. Most of these reactions in biological systems involve large separations (5 to 20 Å) and therefore have a very weak tunneling coupling between the donor (D) and the acceptor (A) sites. This coupling is called the electronic matrix element (T_{DA}). In this weak coupling regime, the ET rates are the product of the square of T_{DA} , as expected from perturbation theory and the probability of the donor and acceptor forming a resonant activated complex (Marcus theory) (1–5). About a decade ago, Beratan and Onuchic developed the Pathways method to estimate these T_{DA} 's and to understand the tunneling mechanism in proteins. The Pathways method assumes that tunneling occurs via a dominant pathway tube (a family of similar pathways, and that the decay through this tube can be quantified as a product of contributions from covalent bonds, hydrogen bonds, and through-space jumps (6, 7). This approach has been widely used by the experimental community (2, 3, 8). However, the Pathways method has two major limitations: It does not include the possibility of interference among multiple paths, and the paths are determined with the “frozen” (crystallographic) protein structure, without accounting for protein motions.

In this report, we go beyond the Pathways method. Our results show that for ET reactions

dominated by a single pathway tube (or a few tubes that interfere constructively), corrections due to protein dynamics are minor. The situation reverses when the assumption of a single pathway tube breaks down, and ET involves multiple tubes with destructive interference. T_{DA} 's are now sensitive to conformational details and nuclear dynamics. Calculations with a single frozen conformation provide an incorrect answer: Tunneling is controlled by far-from-equilibrium protein conformations, where one or few tubes dominate, thereby minimizing destructive interference.

To demonstrate this concept, the dynamical effects on T_{DA} in a bacterial photosynthetic reaction center (BPRC) are explored. The BPRC is a large transmembrane protein-cofactor complex that mediates electron and proton transfer reactions that convert light into chemical energy (9–16). We investigate the ET reactions from the pheophytin (B_{ph}) to the primary quinone (Q_A) and from the latter to the secondary quinone (Q_B), with a focus on the effects of local nuclear dynamics. Although dynamical effects on T_{DA} have been observed in previous calculations (17–19), no consistent theoretical approach has been developed yet. We provide a quantitative description of this new mechanism of dynamic control, which we name dynamical amplification. We also discuss another dynamical control mechanism, conformational gating, which was recently suggested from a high-resolution x-ray analysis of BPRC (9). That analysis revealed that the transition from the dark structure (Q_B in its neutral form) to the light structure (negatively charged Q_B^-) consists mostly of flipping and moving of the

Q_B ring in its binding pocket (10). We show that both dynamical amplification and conformational gating are critical in providing efficient electron transfer between the quinones.

For both the dark and the light BPRC structure, T_{DA} calculations were performed with the Green's function technique (to quantify the electron tunneling propagation through the protein) with a standard extended Huckel electronic Hamiltonian in a bonding and antibonding orbital basis (5, 20, 21). The calculations included B_{ph} , Q_A , Q_B , the iron ion, and the relevant protein environment (Trp^{L100}, Met^{M256}, Trp^{M252}, Met^{M218}, His^{M219}, His^{L190}, His^{L230}, Glu^{M234}, and His^{M266}; the superscript indicates the BPRC chain and the amino acid position in that chain). To compute the average square effective coupling $\langle T_{DA}^2 \rangle$, the Green's functions were evaluated for several conformations (“snapshots”), which were obtained by using molecular dynamics (MD). In addition, T_{DA} was computed for the crystallographic and the “average” conformations (nuclear coordinates averaged over the MD runs).

The MD simulations were performed for both the dark and the light structures with the consistent valence force field (22) for the BPRC fragment and for all amino acids within 8 Å from it. In this initial analysis, we are mainly interested in demonstrating how competition among different tubes leads to dynamical amplification, and we therefore limited dynamics to small nuclear motions by imposing a set of restraints (23). All backbone atoms were fixed, and all other heavy atoms were pulled to their positions in the crystallographic structure by harmonic restraining forces. By choosing the restraining force constant, we controlled the root mean square deviation (rmsd) of these heavy atoms. The rmsd between the crystallographic and the average conformations was about 0.35 Å, and the rmsd between any snapshot and the average conformation was about 0.25 Å. The structures were first equilibrated for 3 ps, followed by a 15-ps MD run with a 0.5-fs time step. A snapshot conformation was saved every 50 ps, leading to a set of 301 snapshots for each MD run.

To quantitatively describe the degree to which nuclear dynamics affect the effective coupling, we introduced the coherence parameter $C = \langle T_{DA} \rangle^2 / \langle T_{DA}^2 \rangle$. Given that $\langle T_{DA}^2 \rangle = \langle T_{DA} \rangle^2 + \langle \delta T_{DA}^2 \rangle$, where $\langle \delta T_{DA}^2 \rangle$ is the mean square deviation, C falls in the range between zero and one. In the limit where the dynamic variations of the Green's function

Department of Physics, University of California at San Diego, La Jolla, CA 92093–0319, USA.

*To whom correspondence should be addressed. E-mail: jonuchic@ucsd.edu